

---

---

**ATMOSPHERIC RADIATION,  
OPTICAL WEATHER, AND CLIMATE**

---

---

## **Study of the Spatial Distributions of CO<sub>2</sub> and CH<sub>4</sub> in the Surface Air Layer over Western Siberia Using a Mobile Platform**

**M. Yu. Arshinov<sup>a,\*</sup>, B. D. Belan<sup>a,\*\*</sup>, D. K. Davydov<sup>a</sup>, A. V. Kozlov<sup>a</sup>, A. V. Fofonov<sup>a</sup>, and V. G. Arshinova<sup>a</sup>**

<sup>a</sup>*V.E. Zuev Institute of Atmospheric Optics, Siberian Branch, Russian Academy of Sciences, Tomsk, 634055 Russia*

<sup>\*</sup>*e-mail: michael@iao.ru*

<sup>\*\*</sup>*e-mail: bbd@iao.ru*

Received March 19, 2020; revised March 19, 2020; accepted June 15, 2020

**Abstract**—We present the results of a large-scale study of carbon dioxide and methane distributions carried out on the territory of Western Siberia in 2018–2019 using a Picarro G4301 portable gas analyzer. The analysis of the data made it possible to retrieve the spatial distribution of background CO<sub>2</sub> and CH<sub>4</sub> concentrations with a high resolution. The inhomogeneities found in the CO<sub>2</sub> and CH<sub>4</sub> distributions were both due to the effect of ecosystems characteristic for different regions of Western Siberia and to specific features of their seasonal cycles.

*Keywords:* atmospheric composition, greenhouse gases, spatial distribution

**DOI:** 10.1134/S1024856020060056

### INTRODUCTION

At present, one of the most important problems, which the world community referred to the “big challenges,” is global warming and the ensuing environmental change. Global warming was predicted 40 years ago as a possible response of the natural environment to growing anthropogenic emissions of greenhouse gases [1]. In recent years, this phenomenon received one more weighty confirmation of its existence against the background of natural long-term climate oscillations [2, 3]. Its essence is that all previous coolings and warmings were regional; while the present phenomenon encompasses all the globe. Recent estimates of the National Oceanic and Atmospheric Administration (NOAA, United States) suggest that in the period from 1990 to 2018, the radiative forcing by long-lived greenhouse gases (GHGs) had increased by 43%, with CO<sub>2</sub> accounting for 81% of this increase [4]. And GHG emissions do not decline despite all the measures undertaken [5].

The awareness of the world community about the situation motivated the creation of international networks for precision measurements of greenhouse gases. To date, operational instrumentation includes: the Global Carbon Project under the auspices of the World Meteorological Organization (WMO–Global Atmosphere Watch), the Global Monitoring System (NOAA/ESRL), the International Integrated Carbon Observation System (ICOS), and some others [6–8]. They make it possible to study the large-scale spatio-temporal variations in the greenhouse gases. For instance, the authors of work [9] report the nonsyn-

chronicity of temporal variations in the CO<sub>2</sub> concentration in large regions such as Africa and South America. Also, denser networks make it possible to identify mesoscale inhomogeneities in greenhouse gas distribution [10].

The growth of anthropogenic GHG emissions in the atmosphere occurring mainly in big industrial centers and the nonuniformity of land coverage by plants strongly complicate the quantitative estimation of their emission and uptake. Despite the fact that most GHG observation stations are located in background regions, GHG concentrations in continental regions are strongly affected by both anthropogenic and biogenic sources. At the same time, separation of natural and anthropogenic components of the carbon cycle is of key importance for correcting the systems of inverse modeling with the use of the data from in situ measurements [11].

Siberia is one of the key Northern Hemisphere regions, where the most marked climate changes are observed, especially in the Arctic zone [12, 13]. In 2000s, V. E. Zuev Institute of Atmospheric Optics, Siberian Branch, Russian Academy of Sciences (IAO SB RAS), in the framework of international collaboration with the National Institute for Environmental Studies (NIES, Japan), had created on the territory of Siberia the Japan-Russia Siberian Tall Tower Inland Observation Network (JR-STATION) [14]. It covers a substantial part of the Western Siberian Plain between 54.5° and 63.2° N and 62.3° and 85.0° E. The JR-STATION sites are spaced 300 to 900 km away. For a technical servicing of stations most remote from

IAO SB RAS, regular off-site expeditions are organized four times a year: in March, June, August, and October. A distance of  $\sim 7000$  km is traversed in each trip. In this regard, the idea of mounting a portable new-generation G4301 gas concentration analyzer (Picarro Inc., United States) on the expedition vehicle was considered. That made it possible to measure the  $\text{CO}_2$  and  $\text{CH}_4$  concentrations during the journey between the stations with a high spatial resolution. This work is devoted to results of measurements of greenhouse gases on the territory of Western Siberia in the surface air layer during these trips.

## 1. METHODS

A Picarro G4301 analyzer can measure the carbon dioxide and methane concentrations at frequency of 1 Hz with errors of 0.4 ppm and 3 ppb, respectively. The principle of its operation is based on the Cavity Ring-Down Spectroscopy (CRDS) method [15].

### 1.1. Sample Preparation

The  $\text{H}_2\text{O}$  vapors are known to influence the accuracy of measurements by most electrooptical gas analyzers used to measure the concentrations of trace atmospheric gases. The authors of work [16] indicate that spectroscopic methods are sensitive to variations in water vapor content in air due to changes in the degree of pressure broadening of absorption lines used to measure the  $\text{CO}_2$  and  $\text{CH}_4$  concentrations. Most Picarro gas analyzers also measure the water vapor content in air simultaneously with  $\text{CO}_2$ ,  $\text{CH}_4$ ,  $\text{N}_2\text{O}$ , and  $\text{CO}$ ; therefore, a correction for  $\text{H}_2\text{O}$  content in air is used to recalculate the concentrations of these gases in dry air. However, it gives satisfactory results when the volume fraction of water vapor  $< 0.7$  and  $< 0.6\%$  for  $\text{CO}_2$  and  $\text{CH}_4$  [17]. In this regard, authors of work [17] recommend a complete drying of the air sample before supplying it to the gas analyzer. In addition to line broadening processes, changes in the reflection coefficients of multilayer dielectric mirrors can also influence the measurement accuracy, depending on the water vapor content in air analyzed during its passage through the optical cavity [18] owing to penetration of  $\text{H}_2\text{O}$  molecules into the multilayer coating [19].

A system of preliminary preparation of air samples was created to avoid possible effects of the abovementioned factors on accuracy of measurements of the  $\text{CO}_2$  and  $\text{CH}_4$  concentrations when the G4301 gas analyzer is used on the vehicle. It was mainly designed to completely remove moisture from a sample analyzed and to stabilize the pressure at a gas analyzer inlet. The sample preparation system and scheme of arrangement of the air intake device and Picarro G4301 gas analyzer on the Renault Duster vehicle were presented in [20]. The ambient air is transferred from the air intake device to the gas analyzer via a Synflex 1300

tube (6-mm outer diameter, 4-mm inner diameter, EATON Corp., PLC). To reduce the time of pumping via the supply channels and to increase the efficiency of the drying system, we use a preliminary pump (NMP-50, KNF Neuberger GmbH) to inject the sample into a coalescence filter (MC 104-F10, Camozzi Pneumatic LLC), which prevents liquid-water droplets from entering the system. Next, the air analyzed passes through the first stage in which membrane dryer MD-110-72F-4 (Perma Pure LLC) is used to remove water vapor from the air. A constant sample flow rate is ensured by a flow regulator with a throttle valve (AS1001F, SMC Pneumatic Co., Ltd.). Final drying is achieved by mounting a magnesium perchlorate ( $\text{Mg}(\text{ClO}_4)_2$ )-filled interchangeable cartridge to the channel. Immediately before the inlet of the gas analyzer, which has a built-in pump, a three-way connector is mounted for equalizing the pressure by evacuating redundant air through a rotameter used for the initial setting of the airflow rate by the AS1001F regulator. The sample analyzed is transferred from the gas analyzer outlet to the external pipe of Nafion membrane for its purging by dry air to increase its efficiency.

### 1.2. Geopositioning

A GLONASS BU-353 receiver is connected to the gas analyzer to determine the position of vehicle while driving. All parameters measured are recorded using specially created software, enabling the measurements of  $\text{CO}_2$  and  $\text{CH}_4$  concentrations and coordinates of the mobile platform to be real-time coupled in a local MySQL database generated in the computer built into the analyzer. A visual control of measurements is carried out using a tablet computer via a remote desktop connected to the G4301 gas analyzer through a wifi channel.

### 1.3. Calibration and Processing of Data

Immediately before and just after an expedition, the G4301 gas analyzer was calibrated using standard gas mixtures (SGM, Table 1) for determining correction coefficients.

Naturally, most data along the vehicle route were burdened by anthropogenic component (motor vehicle exhausts on motorways); therefore, the “background values” were retrieved using the baseline method during subsequent processing [20]. The baseline value of concentration was determined from its minimal values at the section of the route analyzed. In the cases of heavy-traffic motorways, background values of the  $\text{CO}_2$  and  $\text{CH}_4$  concentrations were obtained through periodic windward deviations from the route. This approach was implemented in [21].

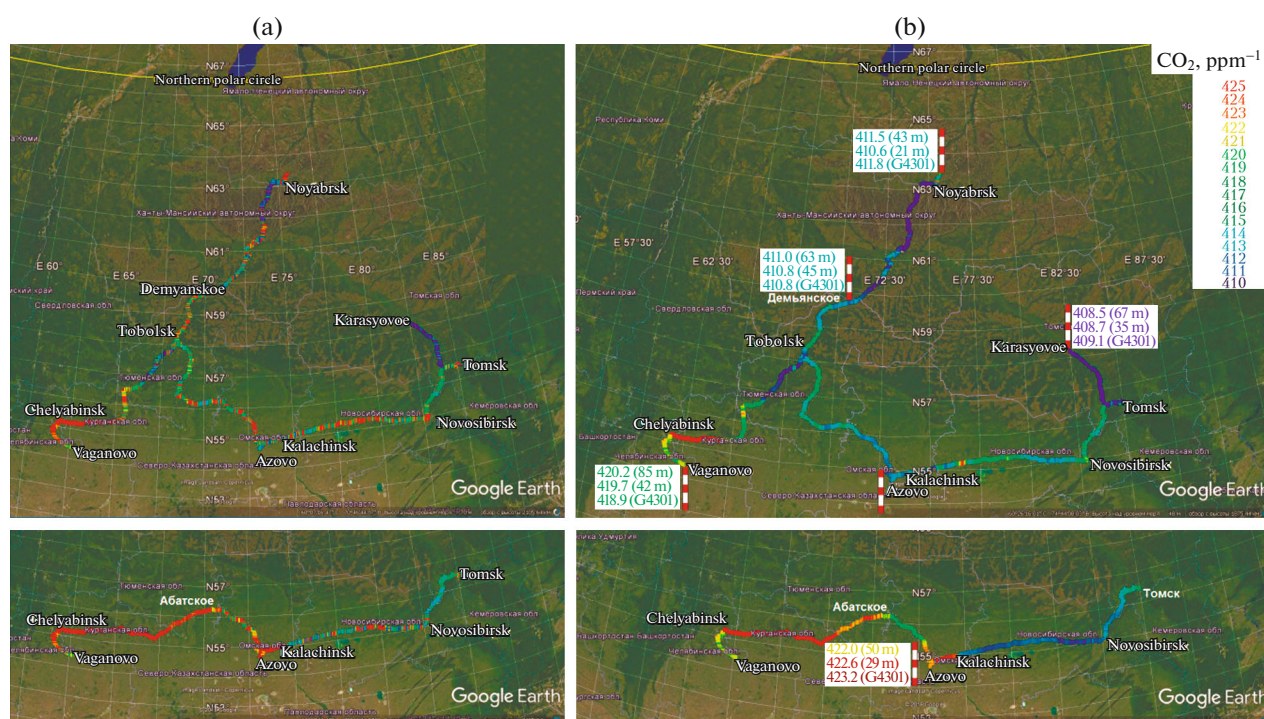


**Fig. 1.** Spatial distribution of CO<sub>2</sub> concentration in the surface air layer of Western Siberia obtained during a mobile campaign in fall 2018 using (a) unfiltered data and (b) background values retrieved by the baseline method; red-white columns correspond to the JR-STATION network sites.

## 2. RESULTS AND DISCUSSION

The inhomogeneities of the spatial distribution of the CO<sub>2</sub> and CH<sub>4</sub> concentrations over the territory of Western Siberia were studied using the Picarro G4301 portable gas analyzer during four mobile campaigns: in late October to early November 2018; March, June, and August 2019.

### 2.1. Spatial Distribution of Carbon Dioxide (fall of 2018)

Figure 1 shows an example of the spatial distribution of carbon dioxide obtained during the first campaign. From Fig. 1a, it can be seen that the most busy motorways are between Novosibirsk, Omsk, and Chelyabinsk, explaining high CO<sub>2</sub> concentrations both at separate sections of the motorway and in the regions of big settlements.

Despite the fact that motor vehicle exhausts strongly affected the measurements, the baseline method made it possible to retrieve the distribution of background

CO<sub>2</sub> concentration in the surface air layer over a considerable part of Western Siberia. For instance, from Fig. 1b, which also presents the CO<sub>2</sub> molar fractions measured at JR-STATION stations and using the mobile complex when visiting them, it can be seen that they agree quite well. The lowest background CO<sub>2</sub> concentrations in October–November 2018 were observed at the sections Tomsk–Karasyovoe, Demyanskoe–Noyabrsk, and Tobolsk–Yalutorovsk (56.7° N, 66.4° E), where the average values had been  $410.1 \pm 1.1$ ,  $410.7 \pm 1.6$ , and  $411.5 \pm 1.5$  ppm, respectively.

The highest background nitrogen dioxide content ( $431.0 \pm 2.2$  ppm) was observed in the western regions between Chelyabinsk and Kurgan, attributed to air mass transport from western regions with high anthropogenic loads and to almost total absence of photosynthetic activity in this period of the year. On the return trip, from Chelyabinsk to Tomsk, the measurements were carried out under conditions determined by a multi-center cyclone with two systems of fronts

**Table 1.** Concentrations of standard gas mixtures and the Picarro G4301 gas analyzer calibration measurements

SGM	CO <sub>2</sub> , ppm	CH <sub>4</sub> , ppb	CO <sub>2</sub> (G4301), ppm	CH <sub>4</sub> (G4301), ppb
No. 1	339.17	1685.17	$335.01 \pm 0.16$	$1669.78 \pm 0.81$
No. 2	365.40	1988.74	$360.78 \pm 0.17$	$1968.74 \pm 0.85$
No. 3	390.24	2283.61	$385.35 \pm 0.17$	$2261.48 \pm 0.86$

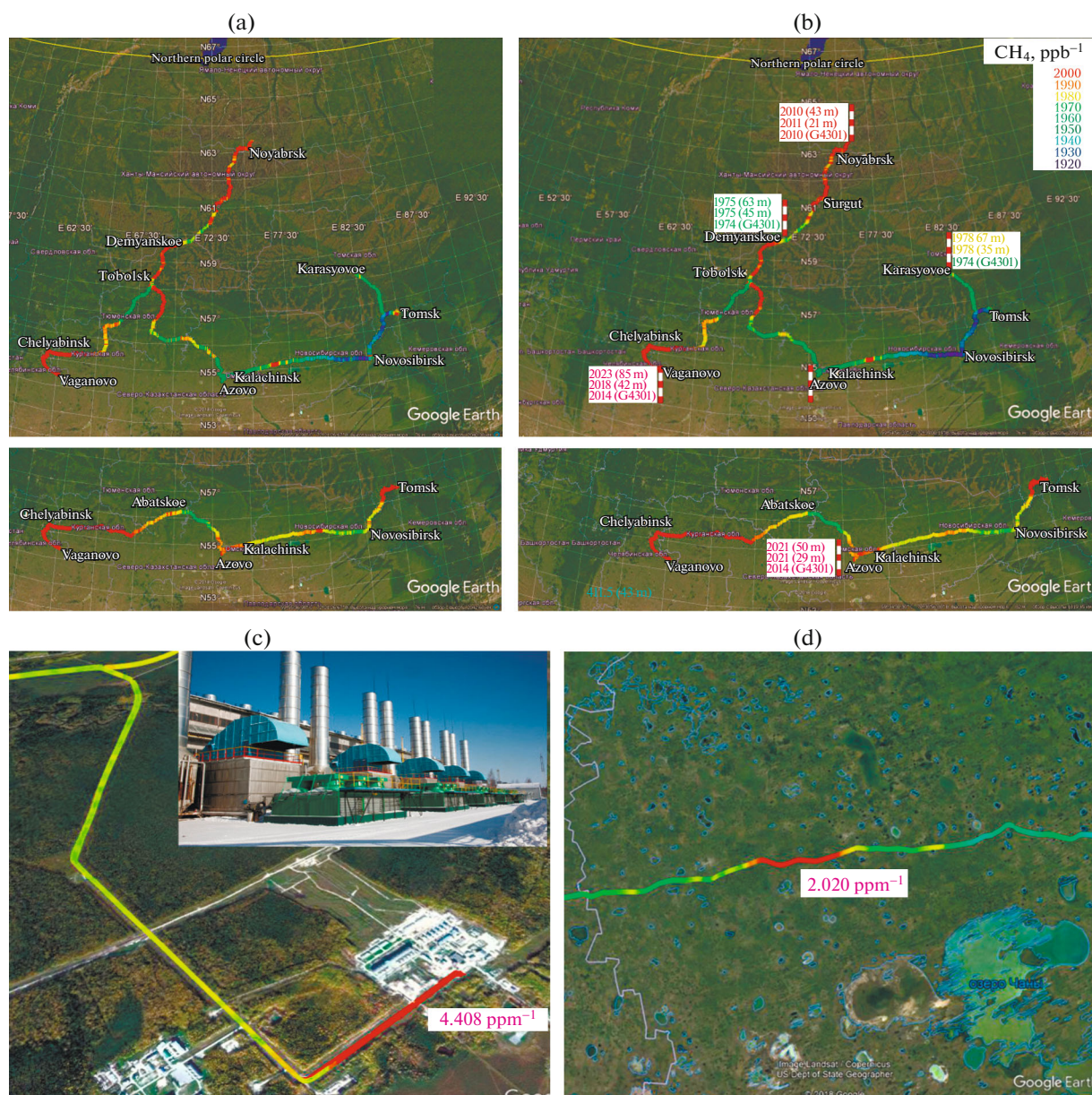


**Fig. 2.** Spatial distribution of the CH<sub>4</sub> concentration in the surface air layer over Western Siberia obtained during mobile campaign in fall 2018 using (a) unfiltered data; (b) background values retrieved by the baseline method, (c) near gas pipeline compressor station CS-6 of Samson local operations and maintenance department for main gas pipelines of JSC Gazprom, and (d) in the wetland area in the Chany region of Novosibirsk region.

covering almost all the territory of Western Siberia. One of the centers of the cyclone was southward of Norilsk, and the other in the region of Khanty-Mansiysk. The axis of the trough stretched from northeast to southwest. The vehicle moved in a warm subtropical air mass between Chelyabinsk and Omsk. In the region of Kalachinsk (75 km east of Omsk), the vehicle crossed the system of fronts and the ambient air temperature sharply dropped, and the further measurements were then carried out in the Arctic air mass with predominant northerly winds. As a result, the CO<sub>2</sub> concentration was found to rapidly decrease, and its average background

value at the section from Kalachinsk to Tomsk had been  $412.7 \pm 1.3$  ppm.

## 2.2. Spatial Distribution of Methane (Fall 2018)

The spatial distribution of methane concentration in Western Siberia in October–November 2018 is presented in Fig. 2. It is characterized by a pronounced positive latitudinal gradient of the CH<sub>4</sub> concentration from steppe regions in the south to wetland territories in the north. In contrast to carbon dioxide, no significant effect of motor vehicles on the measurements of

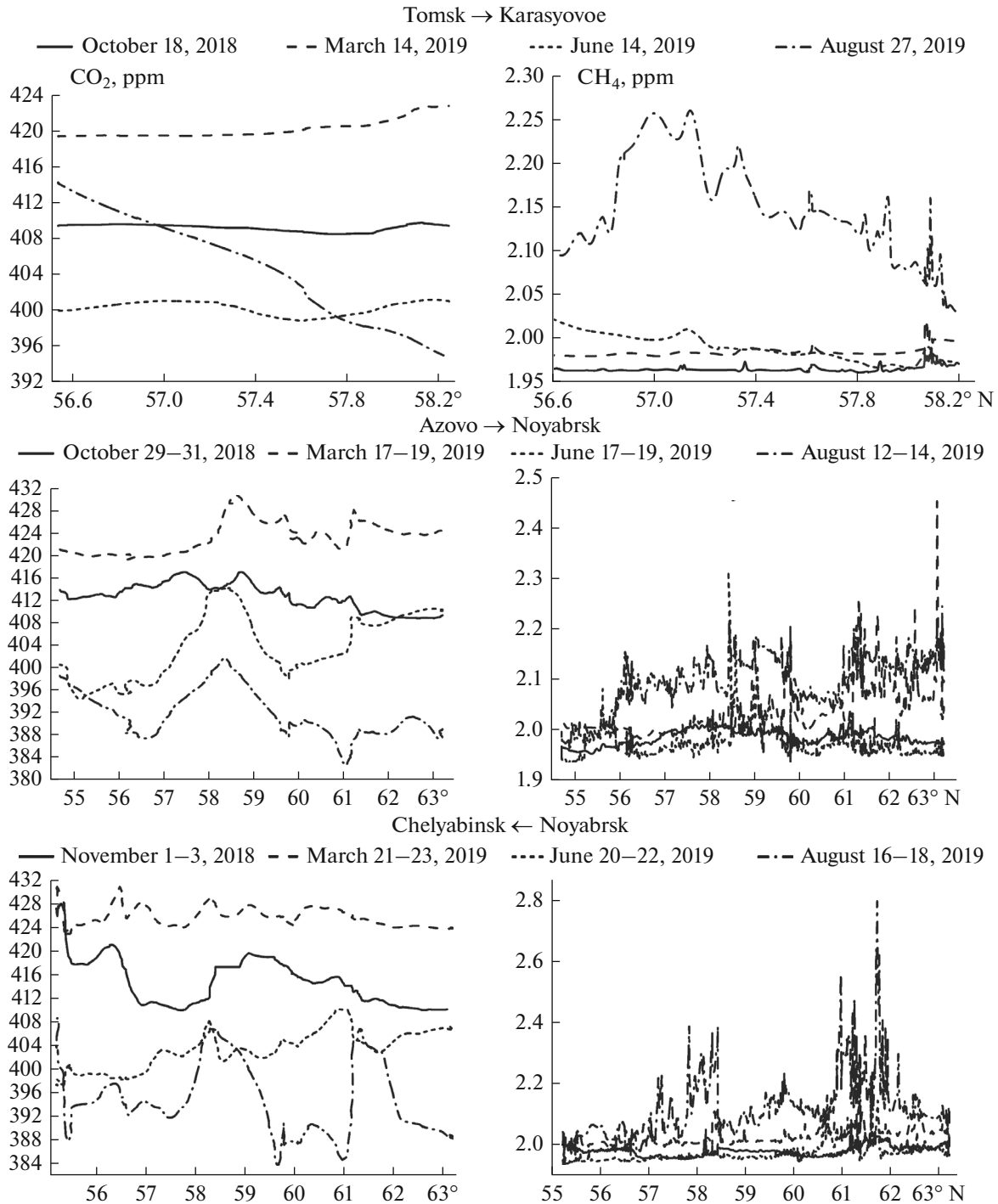


**Fig. 3.** Latitudinal and longitudinal transects of background CO<sub>2</sub> and CH<sub>4</sub> concentrations in the surface air layer over Western Siberia.

methane concentration was observed. The main bursts of methane concentration, much exceeding 2.0 ppm, were recorded in oil and gas production regions, near gas transmission systems and gas stations selling methane as motor fuel. In particular, the absolute maximum (4.408 ppm) was recorded in the immediate vicinity of the gas pipeline compressor station CS-6 of

the Samson local operations and maintenance department for the main gas pipelines of JSC Gazprom (Fig. 2a), located 30 km northeast of the Demyanskoe observation station.

As in the case with carbon dioxide, the high background level of CH<sub>4</sub> molar fraction in the southern regions was observed on extended segment of the route

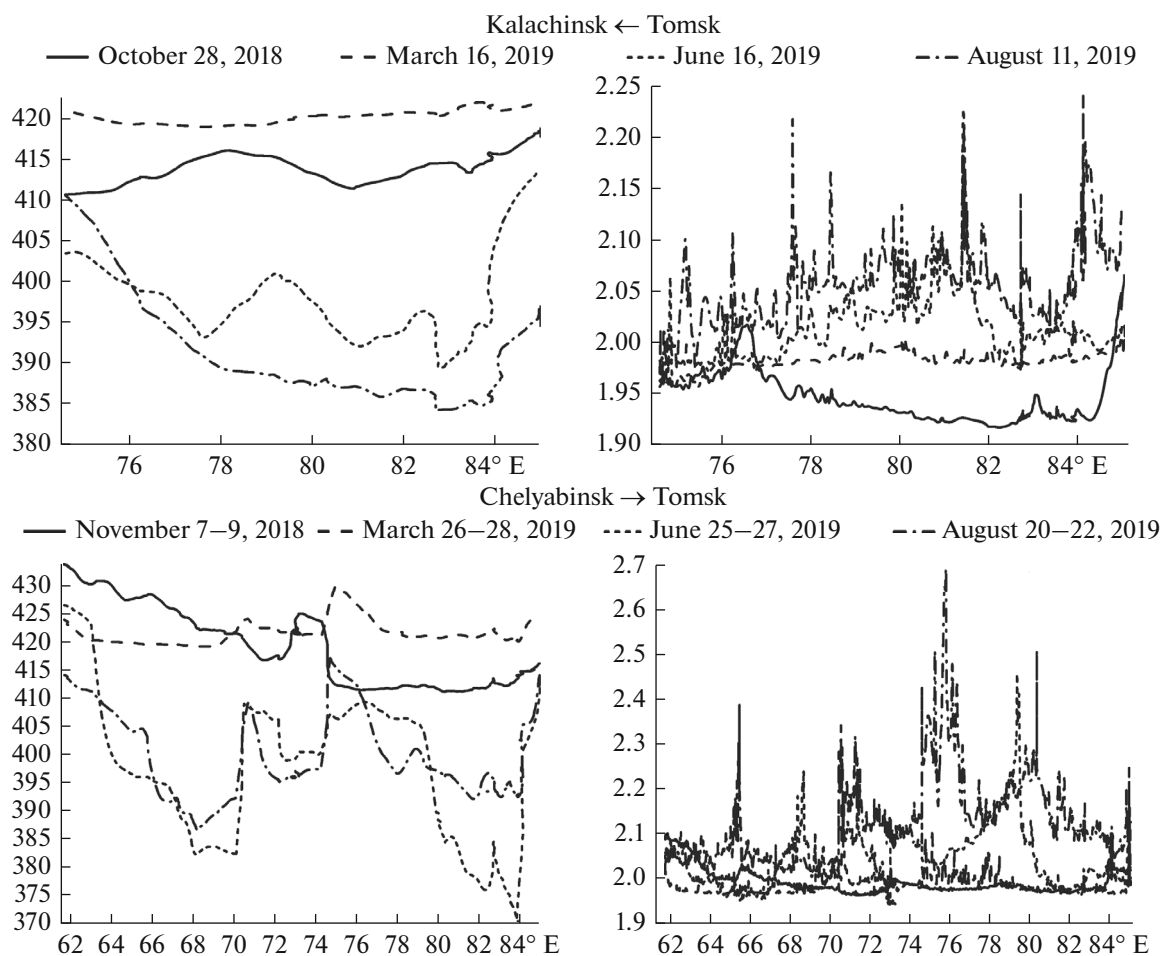


Fig. 3. (Contd.)

between Chelyabinsk and Kurgan, thus proving that the changes happened in air mass with a heavy anthropogenic load.

Further increased concentrations of methane, but now of natural origin, were recorded on October 28, 2018, during motor vehicle trip through the wetlands in the Chany region of Novosibirsk oblast along the route Tomsk–Omsk (Fig. 2b). Eleven days later, on the return trip, the lakes and bogs in this region were already covered by ice, so that methane emission from these water bodies had no effect on the measurements. High background concentrations in this same region were recorded again during the June and August 2019 campaigns, with the  $\text{CH}_4$  molar fraction found to exceed 2.5 ppm during the latter.

### 2.3. Seasonal Variations in the Spatial $\text{CO}_2$ and $\text{CH}_4$ Distributions

The four campaigns allowed us to retrieve the pattern of the seasonal variations in background  $\text{CO}_2$  and  $\text{CH}_4$  concentrations in the surface air layer over the

vast regions of Western Siberia. Their latitudinal and longitudinal transects are presented in Fig. 3.

The  $\text{CO}_2$  and  $\text{CH}_4$  concentrations averaged for each of the transects (Fig. 4 and Table 2) indicate that the maximal  $\text{CO}_2$  levels were observed in March 2019. We should also note that the  $\text{CO}_2$  distribution in the surface air layer of Western Siberia was relatively uniform and the interquartile range (IQR) of  $\text{CO}_2$  molar fractions in each transect was narrow in the cold period of the year (in October and March). This is because of almost no diurnal variation in this period owing to less intense vertical mixing of the atmosphere and weak ecosystem exchange; while the background carbon dioxide content in the atmosphere of the region is determined mainly by the prehistory of the air mass in which measurements are performed.

Data obtained in June and August 2019 were more difficult to analyze because diurnal  $\text{CO}_2$  dynamics were superimposed on measurements carried out along the route, resulting in higher IQR values. However, after compiling a sample of daytime values, when the lower air layers are well mixed and there is an

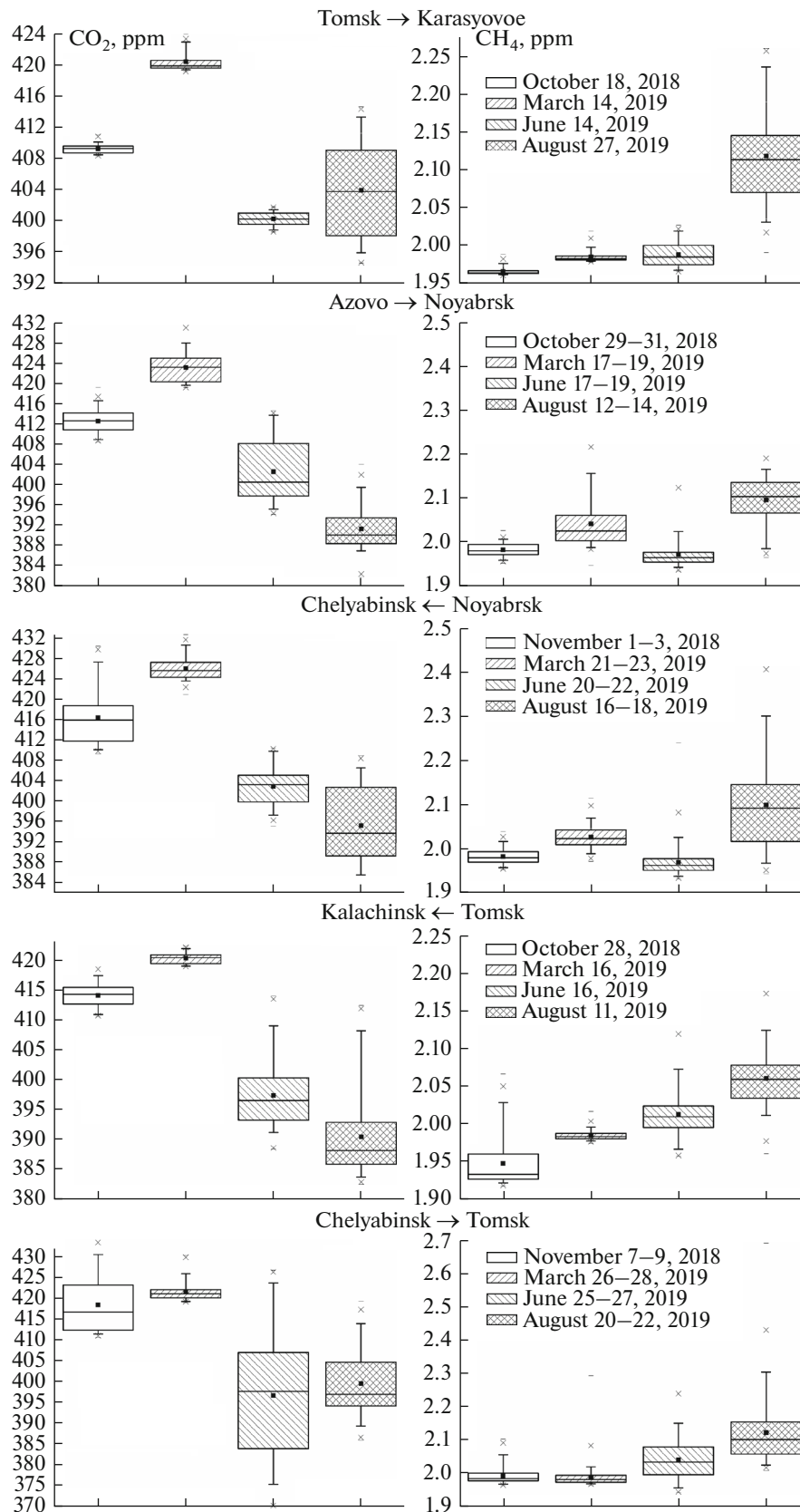


**Fig. 4.** Diagram of the span of background CO<sub>2</sub> and CH<sub>4</sub> concentrations plotted on the basis of statistical analysis of data presented in Fig. 3. Upper and lower boundaries of the boxes are the third and first quartiles, respectively; black square and horizontal line inside the rectangle are the average and median; “—” are the minimal and maximal values of the sample; “x” is the 1st and 99th percentiles; and boundaries of the upper and lower error bars are 1.5 IQR.

**Table 2.** The CO<sub>2</sub> and CH<sub>4</sub> concentrations averaged for each transect and for the territory of Western Siberia covered by mobile measurements

Transect (extents)	Date	CO <sub>2</sub> , ppm			CH <sub>4</sub> , ppb		
		average	IQR	median	average	IQR	median
Tomsk–Karasyovoe (310 km)	Oct 18, 2018	409.2 ± 0.5	0.9	409.2	1966.5 ± 4.7	3.7	1964.4
	Mar 14, 2019	420.4 ± 1.1	1.0	419.8	1985.7 ± 6.7	5.3	1983.4
	Jun 14, 2019	400.2 ± 0.9	1.4	400.2	1988.8 ± 15.8	25.7	1985.7
	Aug 27, 2019	403.9 ± 5.8	10.9	403.7	2118.0 ± 59.6	74.7	2113.4
Azovo–Noyabrsk (1590 km)	Oct 29–31, 2018	412.5 ± 2.3	3.3	412.6	1981.8 ± 15.1	23.3	1979.3
	Mar 17–19, 2019	423.1 ± 2.9	4.6	423.1	2040.9 ± 54.2	57.5	2025.2
	Jun 17–19, 2019	402.6 ± 5.8	10.4	400.5	1971.0 ± 34.5	22.7	1963.8
	Aug 12–14, 2019	391.3 ± 4.1	5.1	390.1	2095.5 ± 51.9	70.2	2103.1
Noyabrsk–Chelyabinsk (1500 km)	Nov 1–3, 2018	416.4 ± 5.1	6.9	415.9	1984.1 ± 17.5	23.4	1981.3
	Mar 21–23, 2019	426.0 ± 2.2	2.9	425.6	2028.0 ± 24.7	33.3	2024.7
	Jun 20–22, 2019	402.9 ± 3.6	5.2	403.3	1971.1 ± 29.4	26.8	1964.1
	Aug 16–18, 2019	395.2 ± 7.1	13.5	393.7	2100.2 ± 104.3	128.8	2093.3
Tomsk–Kalachinsk (820 km)	Oct 28, 2018	414.1 ± 1.9	2.8	414.3	1947.7 ± 31.4	33.1	1933.4
	Mar 16, 2019	420.3 ± 0.9	1.5	420.4	1984.5 ± 5.8	7.1	1983.2
	Jun 16, 2019	397.4 ± 5.4	7.1	396.5	2012.9 ± 32.0	28.9	2009.4
	Aug 11, 2019	390.4 ± 6.6	7.0	388.2	2060.1 ± 36.0	43.7	2058.8
Chelyabinsk–Tomsk (1850 km)	Nov 7–9, 2018	418.4 ± 6.5	10.8	416.7	1993.0 ± 25.8	23.1	1984.5
	Mar 26–28, 2019	421.5 ± 2.1	2.0	421.1	1987.4 ± 24.0	21.0	1981.8
	Jun 25–27, 2019	396.5 ± 13.7	23.1	397.5	2040.5 ± 63.8	83.3	2033.4
	Aug 20–22, 2019	399.4 ± 7.6	10.6	396.9	2120.8 ± 90.6	95.8	2100.6
Western Siberia	Oct 18–Nov 9, 2018	415.6 ± 5.4	5.9	414.1	1980.5 ± 26.69	26.1	1979.4
	Mar 14–28, 2019	422.9 ± 3.0	4.6	422.0	2011.4 ± 41.23	46.8	2000.5
	Jun 14–27, 2019	400.0 ± 9.1	9.5	400.5	1999.2 ± 54.18	58.9	1982.7
	11–28, 2019	395.1 ± 7.6	10.6	393.4	2100.5 ± 81.7	084.6	2090.2

intense uptake of carbon dioxide by ecosystems, the latitudinal CO<sub>2</sub> distribution can be seen to become more uneven after resumed photosynthesis in the growing season (June measurement campaign). For instance, from Figs. 3 and 4 it can be seen that along the sections of the routes Azovo–Noyabrsk and Noyabrsk–Chelyabinsk, a positive latitudinal gradient from southern toward northern regions was clearly manifested, attributed to the delayed onset of the growing period in the latter. This gradient markedly weakens toward August.

In contrast to CO<sub>2</sub>, the distribution of CH<sub>4</sub> had a more complex spatial and seasonal structures. For instance, in October 2018, the spatial distribution over the entire territory was quite uniform, with concentration levels not exceeding 2.0 ppm. That was because there was already almost no biogenic emission of methane in the region under study by that time; and its accumulation in the thin surface atmo-

spheric layer due to anthropogenic emissions was as yet not sufficiently strong.

In March 2019, the anthropogenic component became more marked in all regions, and especially in oil and gas production areas (from Tobolsk to Noyabrsk).

The pattern reversed in June. Resumed biogenic emission in warm southern regions led to higher methane concentrations than in northern areas.

Toward August, the CH<sub>4</sub> concentrations exceeded 2.0 ppm on almost all the territory of Western Siberia, except in steppe regions. It is noteworthy that the spatial distribution in the northern regions became less uniform, seemingly due to different strengths of methane emissions by different boggy ecosystems in and around the Vasyugan Swamp.

The high level of methane content in Tomsk oblast during August was also affected by emissions from forest fires that burned both on the territory of Tomsk region and in Eastern Siberia.

On one hand, our data confirm the results from previous research in this region [10, 22–25]; on the other hand, they confirm the results of measurements in other regions [26–28]. At the same time, measurements from the mobile platform make it possible to identify mesoscale inhomogeneities in the distribution of GHG concentration caused by natural or anthropogenic sources.

## CONCLUSIONS

Measurements of CO<sub>2</sub> and CH<sub>4</sub> concentrations in Western Siberia carried out in 2018–2019 from the mobile platform allowed us to retrieve for the first time the pattern of their spatial distribution with a high spatial resolution, and to identify its seasonal features. Analysis of the results shows the presence of both a latitudinal gradient and mesoscale inhomogeneities in the spatial distribution of greenhouse gases, especially methane. The median values of concentrations observed over Western Siberia in late October to early November 2018, March, June, and August 2019 had been:

—for CO<sub>2</sub>: 414.1, 422.0, 400.5, and 393.4 ppm, respectively;

—for CH<sub>4</sub>: 1979.4, 2000.5, 1982.7, and 2090.2 ppb, respectively.

The data obtained during mobile campaigns can be used to estimate the strength of anthropogenic and natural CO<sub>2</sub> and CH<sub>4</sub> sources, and to model the carbon budget of Siberian ecosystems. In future, we plan to continue the measurements of greenhouse gas concentrations with the portable gas analyzer for determining interannual variations in greenhouse gas content in the atmosphere of Western Siberia.

## FUNDING

This work was carried out within the State Assignment for IAO SB RAS project no. AAAA-A17-117021310142-5.

## CONFLICT OF INTEREST

The authors declare that they have no conflicts of interest.

## REFERENCES

1. M. McNutt, “Times’s up, CO<sub>2</sub>,” *Science* **365** (6432), 411 (2019).
2. S. S. George, “Aberrant synchrony of present-day warming,” *Nature* **571** (7766), 481–482 (2019).
3. R. Neukom, N. Steiger, J. J. Gomez-Navarro, J. Wang, and J. P. Werner, “No evidence for globally coherent warm and cold periods over the preindustrial common era,” *Nature* **571** (7766), 550–554 (2019).
4. *WMO Greenhouse Gas Bulletin* (WMO, Geneva, Switzerland, 2019), vol. 15.
5. N. Hohne, M. Elzen, J. Rogelj, B. Metz, T. Fransen, T. Kuramochi, A. Olhoff, J. Alcamo, H. Winkler, S. Fu, M. Schaeffer, R. Schaeffer, G. P. Peters, S. Maxwell, and N. K. Dubash, “Emissions: World has four times the work or one-third of the time,” *Nature* **579** (7797), 25–28 (2020).
6. *Workshop Proceedings of the 6th WMO/IAEA Meeting on Carbon Dioxide, Other Greenhouse Gases, and Related Measurement Techniques (GGMT-2011)*, Wellington, New Zealand, October 25–28, 2011. *GAW Report No 206* (WMO, 2012).
7. A. E. Andrews, J. D. Kofler, M. E. Trudeau, J. C. Williams, D. H. Neff, K. A. Masarie, D. Y. Chao, D. R. Kitzis, P. C. Novelli, C. L. Zhao, E. J. Dlugokencky, P. M. Lang, M. J. Crotwell, M. L. Fischer, M. J. Parker, J. T. Lee, D. D. Baumann, A. R. Desai, C. O. Stanier, S. F. J. De Wekker, D. E. Wolfe, J. W. Munger, and P. P. Tans, “CO<sub>2</sub>, CO, and CH<sub>4</sub> measurements from tall towers in the NOAA Earth System Research Laboratory’s Global Greenhouse Gas Reference Network: Instrumentation, uncertainty analysis, and recommendations for future high-accuracy greenhouse gas monitoring efforts,” *Atmos. Meas. Tech.* **7** (2), 647–687 (2014).  
<https://doi.org/10.5194/amt-7-647-2014>
8. <http://www.icos-infrastructure.eu/node/15/>. Cited February 19, 2020.
9. A. Rammig, “Tropical carbon sinks are out of sync,” *Nature* **579** (7797), 38–39 (2020).
10. D. Belikov, M. Arshinov, B. Belan, D. Davydov, A. Fofonov, M. Sasakawa, and T. Machida, “Analysis of the diurnal, weekly, and seasonal cycles and annual trends in atmospheric CO<sub>2</sub> and CH<sub>4</sub> at tower network in Siberia from 2005 to 2016,” *Atmosphere* **10** (11), 689 (2019).  
<https://doi.org/10.3390/atmos10110689>
11. A. Schmidt, C. W. Rella, M. Gockede, C. Hanson, Z. Yang, and B. E. Law, “Removing traffic emissions from CO<sub>2</sub> time series measured at a tall tower using mobile measurements and transport modeling,” *Atmos. Environ.* **97**, 94–108 (2014).
12. T. G. Shepherd, “Effects of a warming Arctic,” *Science* **353** (6303), 989–990 (2016).
13. O. M. Johannessen, S. I. Kuzmina, L. P. Bobylev, and M. W. Miles, “Surface air temperature variability and trends in the Arctic: New amplification assessment and regionalisation,” *Tellus A* **68** (2016).  
<https://doi.org/10.3402/tellusa.v68.28234>
14. M. Sasakawa, K. Shimoyama, T. Machida, N. Tsuda, H. Suto, M. Arshinov, D. Davidov, A. Fofonov, O. Krasnov, T. Saeki, Y. Koyama, and S. Maksyutov, “Continuous measurement of methane concentration using 9-tower network over Siberia,” *Tellus B* **62** (5), 403–416 (2010).
15. E. R. Crosson, “A cavity ring-down analyzer for measuring atmospheric levels of methane, carbon dioxide, and water vapor,” *Appl. Phys. B* **92** (3), 403–408 (2008).
16. H. Chen, J. Winderlich, C. Gerbig, A. Hofer, C. W. Rella, E. R. Crosson, A. D. Van Pelt, J. Steinbach, O. Kolle, V. Beck, B. C. Daube, E. W. Gottlieb, V. Y. Chow, G. W. Santoni, and S. C. Wofsy, “High-accuracy continuous airborne measurements of greenhouse gases (CO<sub>2</sub> and CH<sub>4</sub>) using the cavity ring-down spec-

- troscopy (CRDS) technique,” *Atmos. Meas. Tech.* **3** (2), 375–386 (2010).
17. H. Nara, H. Tanimoto, Y. Tohjima, H. Mukai, Y. Nojiri, K. Katsumata, and C. W. Rella, “Effect of air composition ( $N_2$ ,  $O_2$ , Ar, and  $H_2O$ ) on  $CO_2$  and  $CH_4$  measurement by wavelength-scanned cavity ring-down spectroscopy: Calibration and measurement strategy,” *Atmos. Meas. Tech.* **5** (11), 2689–2701 (2012).
  18. L. N. Sinita, A. A. Lugovskoi, V. I. Serdyukov, and M. Yu. Arshinov, “Changes in the multilayer dielectric coating reflection coefficient under variation in the medium humidity,” *Atmos. Ocean. Opt.* **31** (6), 574–581 (2018).
  19. V. I. Serdyukov, L. N. Sinita, and A. A. Lugovskoi, “Influence of gas humidity on the reflection coefficient of multilayer dielectric mirrors,” *Appl. Opt.* **55** (17), 4763–4768 (2016).
  20. M. Yu. Arshinov, B. D. Belan, D. K. Davydov, A. V. Kozlov, A. V. Fofonov, and V. G. Arshinova, “Heterogeneity of the spatial distribution of  $CO_2$  and  $CH_4$  concentrations in the atmospheric surface layer over West Siberia: October–November 2018,” *Proc. SPIE—Int. Soc. Opt. Eng.* **11208** (2019).
  21. I. A. Perez, M. L. Sanchez, M. A. Garcia, and N. Parado, “An experimental relationship between airflow and carbon dioxide concentrations at a rural site,” *Sci. Total Environ.* **533**, 432–438 (2015).
  22. O. Yu. Antokhina, P. N. Antokhin, V. G. Arshinova, M. Yu. Arshinov, B. D. Belan, S. B. Belan, D. K. Davydov, N. V. Dudorova, G. A. Ivlev, A. V. Kozlov, T. M. Rasskazchikova, D. E. Savkin, D. V. Simonenkov, T. K. Sklyadneva, G. N. Tolmachev, and A. V. Fofonov, “Study of air composition in different air masses,” *Atmos. Ocean. Opt.* **32** (1), 72–79 (2019).
  23. M. Yu. Arshinov, B. D. Belan, D. K. Davydov, O. A. Krasnov, Sh. Sh. Macsutov, T. Machida, M. Sasakawa, and A. V. Fofonov, “Organic aerosol in air of Siberia and the Arctic. Part 1. Geographic features and temporal dynamics,” *Opt. Atmos. Okeana* **31** (8), 670–681 (2018).
  24. O. Yu. Antokhina, P. N. Antokhin, V. G. Arshinova, M. Yu. Arshinov, B. D. Belan, S. B. Belan, D. K. Davydov, N. V. Dudorova, G. A. Ivlev, A. V. Kozlov, O. A. Krasnov, Sh. Sh. Maksyutov, T. Machida, M. V. Panchenko, D. A. Pestunov, T. M. Rasskazchikova, D. E. Savkin, Motoki, Sasakawa, D. V. Simonenkov, T. K. Sklyadneva, G. N. Tolmachev, and A. V. Fofonov, “Dynamics of the greenhouse gas concentrations in Western Siberia,” *Opt. Atmos. Okeana* **32** (9), 777–785 (2019).
  25. A. V. Timokhina, A. S. Prokushkin, A. V. Panov, R. A. Kolosov, N. V. Sidenko, I. Lavrich, and M. Khaimann, “Interannual variability of atmospheric  $CO_2$  concentrations over central Siberia from ZOTTO data for 2009–2015,” *Rus. Meteorol. Hydrol.* **43** (5), 288–294 (2015).
  26. P. Friedlingstein, M. W. Jones, M. O’ Sullivan, R. M. Andrew, J. Hauck, G. P. Peters, W. Peters, J. Pongratz, S. Sitch, C. Le Quere, D. C. E. Bakker, J. G. Canadell, P. Ciais, R. B. Jackson, P. Anthoni, L. Barbero, A. Bastos, V. Bastrikov, M. Becker, L. Bopp, E. Buitenhuis, N. Chandra, F. Chevallier, L. P. Chini, K. I. Currie, R. A. Feely, M. Gehlen, D. Gilfillan, T. Gkritzalis, D. S. Goll, N. Gruber, S. Gutekunst, I. Harris, V. Haverd, R. A. Houghton, G. Hurtt, T. Ilyina, A. K. Jain, E. Joetzer, J. O. Kaplan, E. Kato, K. K. Goldewijk, J. I. Korsbakken, P. Landschutner, S. K. Lauvset, N. Lefevre, A. Lenton, S. Lienert, D. Lombardozzi, G. Marland, P. C. McGuire, J. R. Melton, N. Metzl, D. R. Munro, J. E. M. S. Nabel, S.-I. Nakaoka, C. Neill, A. M. Omar, T. Ono, A. Peregon, D. Pierrot, B. Poulter, G. Rehder, L. Resplandy, E. Robertson, C. Rodenbeck, R. Seferian, J. Schwinger, N. Smith, P. P. Tans, H. Tian, B. Tilbrook, F. N. Tubiello, G. R. van der Werf, A. J. Wiltshire, and S. Zaehle, “Global carbon budget 2019,” *Earth Syst. Sci. Data* **11** (4), 1783–1838 (2019).
  27. A. Krasnova, M. Kukumagi, U. Mander, R. Torga, D. Krasnov, S. M. Noe, I. Ostonen, U. Puttsepp, H. Killian, V. Uri, K. Lohmus, J. Sober, and K. Soosaar, “Carbon exchange in a hemiboreal mixed forest in relation to tree species composition,” *Agric. For. Meteorol.* **275**, 11–23 (2019).
  28. M. Korkiakoski, J.-P. Tuovinen, T. Penttila, S. Sarkkola, P. Ojanen, K. Minkkinen, J. Rainne, T. Laurila, and A. Lohila, “Greenhouse gas and energy fluxes in a boreal peatland forest after clear-cutting,” *Biogeosciences* **16** (19), 3703–3723 (2019).

*Translated by O. Bazhenov*